A Quantum-Chemistry-Based Potential for a Poly(ester urethane)

Grant D. Smith,* Dmitry Bedrov, Oleksiy Byutner, Oleg Borodin, and Chakravarthy Ayyagari

Department of Materials Science and Engineering and Department of Chemical and Fuels Engineering, 122 South Central Campus Drive, Room 304, University of Utah, Salt Lake City, Utah 84112

Thomas D. Sewell

Theoretical Division, Los Alamos National Laboratory, Los Alamos, New Mexico 87545

Received: November 27, 2002; In Final Form: April 10, 2003

We have carried out extensive high-level quantum chemistry studies of the geometry, charge distribution, conformational energies, and hydrogen-bonding energies of model compounds for a family of Estane thermoplastic urethanes (TPUs). Upon the basis of these studies, we have parametrized a classical potential for use in atomistic simulations of Estane TPUs that can also be applied directly or with minor extensions to a wide variety of polyesters and polyurethanes.

Introduction

Estane thermoplastic polyurethanes (TPUs) are families of poly(ether urethane) and poly(ester urethane) elastomers with excellent abrasion and wear resistance, tensile strength, elongation properties, impact resistance, low-temperature flexibility, and ease of processing.[1,2] Estane TPUs are utilized in a wide variety of applications including biomedical applications[3] (e.g., prosthetics,[4] biodegradable implants,[5] and cardiovascular prostheses[6]), water-permeable membranes,[3] coatings and sheathing,[2,3] and binders for propellants and plastic-bonded explosives (PBXs).[7,8] Estane 5703, a poly(butylene adipate-*co*-tetramethylene diphenyl-urethane) referred to hereafter simply as Estane, shown in Figure 1, is a random copolymer of poly(butylene adipate) (PBA) soft segments formed from adipic acid and 1,4-butanediol (BDO) linkages and poly(tetramethylene diphenylmethane−urethane) (PTDU) hard segments formed by polymerization of bis-1,1′-(methyl phenyl-4-isocyanate) (diphenylmethane diisocyanate or MDI) and BDO. Estane is a major component of the elastomeric binder for various PBXs, including PBX-9501. While the structure and dynamic-mechanical behavior of Estane and related TPUs have been the subject of much experimental investigation, property−structure relationships in these morphologically complex polymers remain poorly understood. It is known that the behavior of TPUs is largely controlled by association and segregation of urethane units that form “hard” domains that act as physical cross-links between “softer” domains.[9] The nanoscale morphology of TPUs, specifically the degree to which the hard and soft segments segregate, the structure of the self-assembled hard domains, and the organization of these domains, plays a vital role in determining the properties of the elastomer.[10]

We believe atomistic simulations can provide badly needed molecular-level understanding of the self-assembly of hard segments in Estane, the resulting domain structure, and the influence of this domain structure on the thermodynamic, mechanical, dynamic, and transport properties of the elastomer. Recently, we have conducted molecular dynamics (MD) simulation studies of self-assembling, coarse-grained polymer solutions that yielded important insights into the relationship between the self-assembled nanostructure, the dynamics of polymers within these domains, the dynamics of the domains, and the viscoelastic response of the polymer.[11] To utilize atomistic MD simulations for analogous studies of Estane, it is imperative that we have an accurate description of polar and hydrogen-bonding interactions between functional groups that drive aggregation of the hard segments, as well as the molecular geometry and conformational energetics of Estane that largely determine static and dynamic properties of the polymer. For this purpose, we have conducted high-level quantum chemistry studies of Estane model compounds at a level of theory equivalent to, or even superior to, that used in our studies of HMX (octahydro-1,3,5,7-tetranitro-1,3,5,7-tetrazocine) model compounds that led to our successful atomistic potential (force field)[12] for that component of PBXs. Subsequently, we utilized that quantum-chemistry-based potential in MD simulations of liquid[13] and crystalline HMX[14] to determine transport, thermodynamic, and mechanical properties over a wide range of $P-T$ conditions. Similar to our efforts for HMX,[12] as well as a variety of polymers,[15−19] we have derived a classical force field for Estane based upon quantum chemistry geometries and energies for Estane model compounds and present the resulting force field here. In future work, we will use this potential in simulation studies of Estane and, in combination with our HMX potential, PBXs.

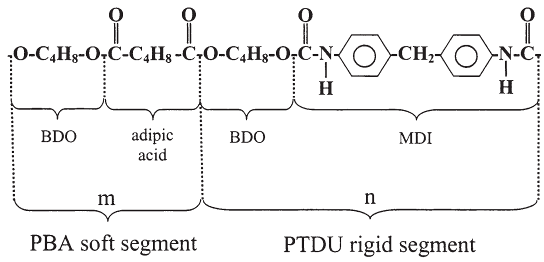

Figure 1. Chemical structure of Estane.

I. Quantum Chemistry Studies of Model Compounds and Complexes for Estane

A. Model Compounds and Complexes. A representative segment of Estane ($m = n = 1$, refer to Figure 1) containing

10.1021/jp0225018 CCC: $25.00
Published on Web 08/27/2003

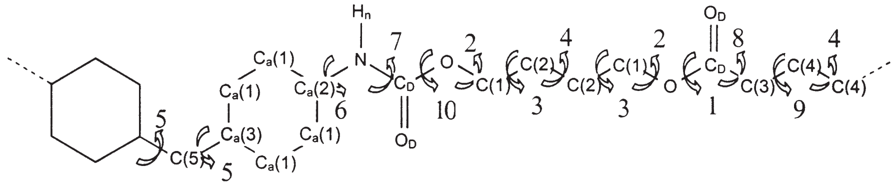

Figure 2. Labeling of unique dihedrals in a representative segment of Estane. All dihedrals are defined on the basis of backbone atoms. Atom types for assigning partial atomic charges (Table 2) are also denoted. Methylene and aromatic hydrogen atoms are not shown.

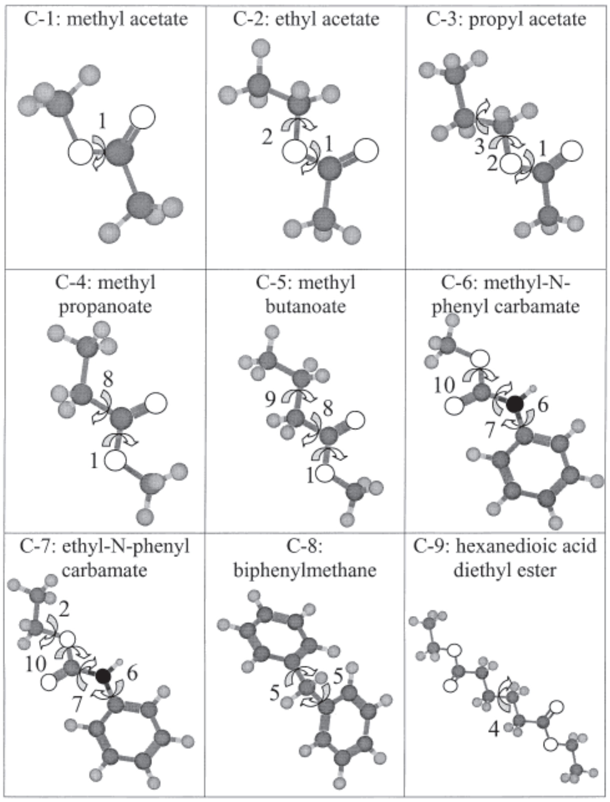

Figure 3. Model Estane compounds showing dihedral types.

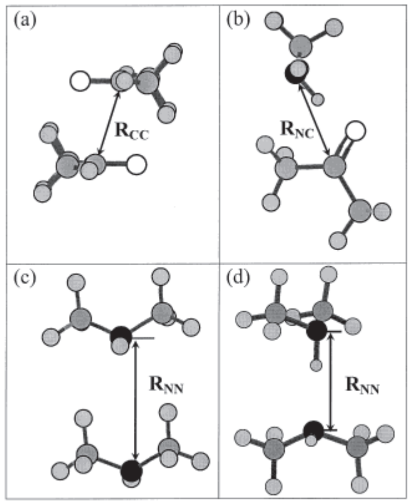

Figure 4. Model complexes for studying polar and hydrogen-bonding interactions in Estane: (a) $(DMK)_2$; (b) DMK−DMA; (c) $(DMA)_2$ non-hydrogen-bonding path; (d) $(DMA)_2$ hydrogen-bonding path. Double-headed arrows indicate the path along which the molecules were moved for generating the binding energy paths shown in Figure 5. The paths are labeled according to the atomic centers terminating the paths (e.g., R_{cc} is the distance between carbonyl carbons in the $(DMK)_2$ complex).

all unique dihedrals (labeled) is shown in Figure 2. This compound is much too large for the high-level quantum chemistry calculations needed to accurately reproduce conformational geometries and energies. As in our previous force field development for HMX and polymers, we have investigated a series of smaller compounds containing the dihedral arrangements present in the polymer. These model compounds are shown in Figure 3. The dihedral(s) examined for each of these compounds is (are) labeled according to its correspondence with the polymer structure (Figure 2).

Where possible, we have taken parameters for nonbonded repulsion/dispersion interactions from our previous quantum-chemistry-based potentials for related polymers. To establish that these parameters, combined with the partial atomic charges obtained from this work, accurately reproduce the strong polar and hydrogen-bonding interactions between Estane functional groups, as well as to determine parameters needed to describe $N\cdots H_n$ hydrogen bonding (see Figure 2 for atom types), which we have not previously considered, we have conducted quantum chemistry studies of the binding energy for dimethyl ketone−dimethyl ketone, dimethyl ketone−dimethylamine, and dimethylamine−dimethylamine or $(DMK)_2$, DMK−DMA, and $(DMA)_2$, respectively, as shown in Figure 4, as a function of intermolecular separation. The quantum chemistry studies of those compounds and complexes and the parametrization of the atomistic potential to accurately reproduce their geometry, conformational energies, electrostatic potentials, and binding energies are described below.

B. Quantum Chemistry Methodology. All ab initio quantum chemistry studies of the Estane model compounds and complexes were performed using Gaussian 98.[20] Initial geometry optimizations of molecular clusters (minimum energy configurations) and Estane model compounds (conformational energy minima and rotational energy barriers) were carried out using density functional theory at the B3LYP[21]/6-31G* level. B3LYP, Hartree−Fock (HF), and MP2 energies were determined with the same basis set using the B3LYP/6-31G* geometries. Subsequent optimization was carried out at the B3LYP/aug-cc-pvdz[22,23] level, again followed by single-point determination of B3LYP, HF, and MP2 energies. The single exception to this procedure was biphenylmethane (Figure 3, compound **C-8**) where B3LYP/cc-pvdz geometries were determined, followed by single-point determination of B3LYP, HF, and MP2 energies with the aug-cc-pvdz basis set. For many compounds (see force field parametrization below), MP2/aug-cc-pvdz energies were also determined at nonstationary points by constraining dihedral angles and optimizing the remaining internal coordinates at the B3LYP/aug-cc-pvdz level. Conformational geometries and energies for the important low-energy conformers and rotational energy barriers (saddle points) for each model compound (Figure 3) are summarized in Table 1 for the larger basis set. Comparison of the B3LYP/6-31G*//MP2/6-31G* (not shown)

TABLE 1: Conformational Geometries and Energies of Important Conformers and Saddle Points for Estane Model Compounds

Methyl Acetate (**C-1**)

state	ϕ_1[a]	B3LYP[b]	ΔE[c]	HF[b]	ΔE[c]	MP2[b]	ΔE[a,c]
min	180.0 (180)	−268.426 150	0.0	−266.871 792	0.0	−267.692 806	0.0 (0.0)
min	0.0 (0)	−268.414 708	7.2	−266.858 020	8.6	−267.681 082	7.4 (7.4)
sad	84.7 (85)	−268.405 189	13.1	−266.851 712	12.6	−267.671 497	13.4 (13.3)

Ethyl Acetate (**C-2**)

state	ϕ_1	ϕ_2	B3LYP	ΔE	HF	ΔE	MP2	ΔE
min	180.0 (180)	180.0 (180)	−307.748 184	0.0	−305.915 572	0.0	−306.884 591	0.0 (0.0)
min	181.0 (179)	86.3 (86)	−307.747 594	0.4	−305.914 476	0.7	−306.884 615	0.0 (0.2)
sad	180.1 (180)	124.2 (127)	−307.746 847	0.8	−305.913 286	1.4	−306.882 772	1.1 (1.2)
sad	180.0 (180)	0.0 (0)	−307.736 432	7.4	−305.902 657	8.1	−306.872 396	7.7 (7.8)

Propyl Acetate (**C-3**)

state	ϕ_1	ϕ_2	ϕ_3	B3LYP	ΔE	HF	ΔE	MP2	ΔE
min	180.6 (179)	88.2 (86)	61.4 (63)	−347.064 384	0.0	−344.952 708	0.0	−346.072 219	0.0 (0.0)
min	180.0 (180)	180.0 (180)	180.0 (180)	−347.065 165	−0.5	−344.954 238	−1.0	−346.071 920	0.2 (0.2)
min	180.9 (180)	86.9 (88)	176.8 (180)	−347.064 752	−0.2	−344.953 284	−0.4	−346.072 239	0.0 (0.2)
min	180.5 (180)	183.0 (182)	65.4 (64)	−347.065 103	−0.5	−344.953 939	−0.8	−346.072 268	0.0 (0.0)
sad	180.0 (180)	180.0 (180)	0.0 (0)	−347.057 226	4.5	−344.945 113	4.7	−346.063 956	5.2 (5.2)
sad	180.0 (180)	179.2 (181)	120.2 (120)	−347.060 254	2.6	−344.948 108	2.8	−346.066 445	3.6 (3.6)

Methyl Propanoate (**C-4**)

state	ϕ_1	ϕ_8	B3LYP	ΔE	HF	ΔE	MP2	ΔE
min	180.0 (180)	180.0 (180)	−307.743 604	0.0	−305.911 037	0.0	−306.880 681	0.0 (0.0)
min	182.5 (183)	91.3 (78)	−307.742 304	0.8	−305.909 354	1.1	−306.879 769	0.6 (0.5)
sad	182.3 (180)	99.1 (106)	−307.742 295	0.8	−305.909 252	1.1	−306.879 752	0.6 (0.6)
sad	180.0 (180)	0.0 (0.0)	−307.741 689	1.2	−305.908 376	1.7	−306.878 879	1.1 (1.1)

Methyl Butanoate (**C-5**)

state	ϕ_1	ϕ_8	ϕ_9	B3LYP	ΔE	HF	ΔE	MP2	ΔE
min	180.0 (180)	180.0 (180)	180.0 (180)		0.0	−344.949 582	−0.4	−346.068 196	0.4 (0.05)
min	182.8 (180)	199.9 (204)	70.1 (64)		0.0	−344.948 957	0.0	−346.068 776	0.0 (0.0)
min	182.5 (180)	91.7 (87)	177.5 (180)		0.0	−344.948 402	0.4	−346.067 994	0.5 (0.8)
min	180.3 (180)	63.1 (73)	61.6 (63)		0.0	−344.947 977	0.6	−346.068 239	0.3 (0.5)
sad	180.1 (180)	180.8 (144)	121.7 (125)	−347.057 048	0.0	−344.944 766	2.6	−346.064 001	3.0 (3.4)
sad	181.7 (180)	92.9 (89)	−1.7 (−1)	−347.052 989	0.0	−344.940 060	5.6	−346.061 901	4.3 (4.3)
sad	182.6 (180)	88.4 (83)	118.3 (119)	−347.055 116	0.0	−344.942 869	3.8	−346.062 729	3.8 (3.3)

Methyl-*N*-phenyl Carbamate (**C-6**)

state	ϕ_6	ϕ_7	ϕ_{10}	B3LYP	ΔE	HF	ΔE	MP2	ΔE
min	180.0 (180)	180.0 (180)	180.0 (180)	−515.559 726	0	−512.451 855	0	−514.101 224	0.0 (0.0)
min	180.0 (180)	180.0 (180)	0.00 (0)	−515.546 418	8.4	−512.435 804	10.1	−514.088 034	8.3 (8.2)
min	180.0 (213)	0.0 (5)	180.0 (180)			−512.447 323	2.8	−514.097 560	2.3 (2.7)
sad	181.3 (181)	180.5 (182)	66.9 (68)	−515.542 688	10.7	−512.433 740	11.4	−514.084 148	10.7 (10.6)
sad	90.0 (90)	180 (180)	180 (180)	−515.552 533	4.5	−512.448 170	2.3	−514.095 656	3.5 (3.2)
sad	91.9 (90)	−1.3 (0)	179.7 (180)			−512.447 441	2.8	−514.095 727	3.5 (3.3)
sad	152.9 (183)	116.1 (102)	178.9 (180)	−515.534 395	15.9	−512.426 135	16.1	−514.077 550	14.9 (16.1)

Ethyl-*N*-phenyl Carbamate (**C-7**)

state	ϕ_7	ϕ_{10}	ϕ_2	B3LYP	ΔE	HF	ΔE	MP2	ΔE
min	179.7 (180)	181.9 (180)	86.5 (86)	−554.881 454	0.0	−551.494 846	0.0	−553.293 527	0.0 (0.1)
min	180.0 (180)	180.0 (180)	180.0 (180)	−554.881 788	−0.2	−551.495 754	−0.6	−553.293 251	0.2 (0.0)
sad	180.0 (180)	180.0 (180)	0.0 (180)	−554.870 281	7.0	−551.482 987	7.4	−553.281 513	7.5 (7.4)
sad	180.2 (180)	179.5 (182)	125.5 (127)	−554.880 704	0.5	−551.493 708	0.7	−553.291 706	1.1 (1.2)

Biphenylmethane (**C-8**)[d]

state	ϕ_5	ϕ_5	B3LYP	ΔE	HF	ΔE	MP2	ΔE
min	56.0 (71)	58.9 (71)	−502.644 342	0.0	−499.334 972	0.0	−501.105 446	0.0 (0.0)
sad	0.0 (0)	90.0 (90)	−502.643 590	0.5	−499.334 356	0.4	−501.105 390	0.1 (0.4)
sad	90.0 (90)	90.0 (90)	−502.643 642	0.4	−499.333 979	0.6	−501.104 594	0.5 (0.2)
sad[e]	0.0	0.0	−502.629 788	9.1	−499.318 194	10.5	−501.088 984	10.4 (11.0)

Hexanedioic Acid Diethyl Ester (**C-9**)

state	ϕ_4	B3LYP	ΔE	HF	ΔE	MP2	ΔE
min	180 (180)	−692.929 016	0.0	−688.749 477	0.0	−690.969 752	0.0 (0.0)
min	66.2 (66)	−692.927 509	1.0	−688.747 465	1.3	−690.968 901	0.5 (0.5)
sad	0.0 (0)	−692.919 493	6.0	−688.738 432	6.9	−690.960 757	5.6 (5.5)
sad	119.1 (121)	−692.924 076	3.1	−688.743 622	3.7	−690.964 496	3.3 (3.3)

[a] Values in parentheses are from molecular mechanics calculations. [b] B3LYP/aug-cc-pvdz geometries, aug-cc-pvdz energies. [c] Relative to the lowest-energy (MP2) conformer, in kcal mol^{-1}. [d] B3LYP/cc-pvdz geometries; aug-cc-pvdz energies. [e] Second-order saddle point.

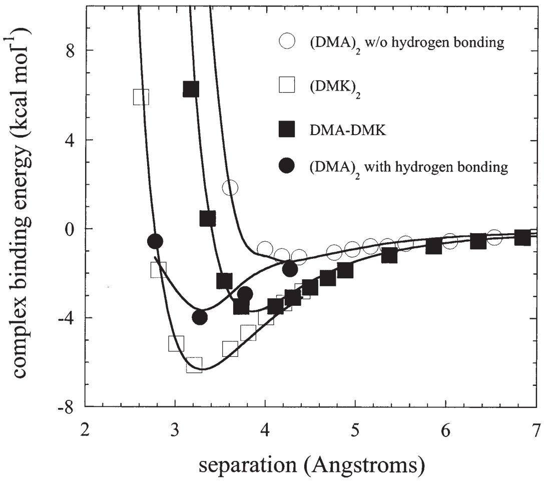

Figure 5. Binding energies for model complexes from quantum chemistry (symbols) and molecular mechanics (solid curves) as a function of intermolecular separation along the paths shown in Figure 4.

and B3LYP/aug-cc-pvdz//MP2/aug-cc-pvdz geometries//energies revealed only small differences in geometries of important conformations of the model compounds but in some cases large (up to 1 kcal mol^{-1}) differences in relative conformational energies. This discrepancy indicates that the larger basis sets are needed to obtain accurate conformational energies for the Estane model compounds. Comparison of MP2 and B3LYP energies for the important conformers of the model compounds (Table 1) reveals differences up to 0.5 kcal mol^{-1} or greater in some cases, indicating that electron correlation effects (i.e., dispersion) not captured by the density functional approach are important in determining relative conformational energies.

The binding energies for the B3LYP/aug-cc-pvdz optimized cluster geometries, shown in Figure 4, were determined at the MP2/aug-cc-pvdz level and were corrected for basis set superposition error (BSSE) using the counterpoise method.[24] The intermolecular spacing was subsequently increased and decreased along the indicated paths while maintaining fixed molecular geometries corresponding to the minimum-energy complex (Figure 4). BSSE-corrected binding energies, given as E_{complex}(MP2/aug-cc-pvdz) $-$ E_1(MP2/aug-cc-pvdz + ghost 2) $-$ E_2(MP2/aug-cc-pvdz + ghost 1), where E_{complex}, E_1, and E_2 are the energies of the complex, molecule 1, and molecule 2, respectively, are shown as a function of separation for the various complexes in Figure 5.

II. Nonbonded Interaction Parameters

A. Partial Atomic Charges for Model Complexes and Compounds. In our potential, all intermolecular and intramolecular polar interactions are represented by Coulomb interactions between partial atomic charges,

$$U^{\mathrm{Coulomb}}(\mathbf{r}) = \sum_{(i,j)} \frac{332.07 q_i q_j}{r_{ij}} \tag{1}$$

where q_i is the charge of atom i, r_{ij} is the separation between atoms i and j and $U^{\mathrm{Coulomb}}(\mathbf{r})$ is the total Coulomb energy in kcal mol^{-1} that depends on the position of all atoms in the system, represented by the vector $\mathbf{r}$. The sum is over all intermolecular pairs and over all intramolecular pairs excluding atoms directly bonded or participating in the same valence bend. Partial atomic charges for the model compounds (DMA, DMK, and those shown in Figure 3) were obtained by determining the set of charges that best reproduce the electrostatic potential for a grid of points surrounding a given molecule in the lowest-energy conformation while at the same time accurately reproducing the molecular dipole moment. The electrostatic potential and molecular dipole moments were obtained from the MP2/aug-cc-pvdz wave functions. The electrostatic grid extended from 1.8 Å for hydrogen atoms, from 2.5 Å for carbon atoms, from 2.0 Å for nitrogen atoms, and from 1.8 Å for oxygen atoms to 3.5 Å from each atom. For each molecule, the electrostatic potential was evaluated at approximately 16 000 points. During the fitting procedure, like atoms within a molecule (e.g., methyl hydrogen atoms) were constrained to have the same charge. The partial atomic charges obtained in this manner for DMA are methyl hydrogen = 0.182, methyl carbon = −0.514, nitrogen = −0.372, and amine hydrogen = 0.308, and those for DMK are methyl hydrogen = 0.182, methyl carbon = −0.713, carbonyl carbon = 0.878, and carbonyl oxygen = −0.544.

The partial atomic charges for the Estane compounds shown in Figure 3 (see Figure 2 for atom and charge types), based upon applying the electrostatic potential method described above for the lowest-energy conformer of each compound (Table 1), are given in Table 2. Partial atomic charges for the polymer (Estane) are also given in Table 2. These were determined by averaging the partial atomic charges for each atom type from the most representative model compounds for that atom type,[25] indicated in bold in Table 2. Minor adjustments were made to the charges to yield charge-neutral PBA and PTDU segments (see Figure 1).

B. Repulsion and Dispersion Interactions. Intermolecular and intramolecular repulsion and dispersion interactions are represented in our potential by

$$U^{\mathrm{rep}}(\mathbf{r}) = \sum_{(i,j)} A_{ij} \exp(-B_{ij} r_{ij}) \tag{2}$$

$$U^{\mathrm{disp}}(\mathbf{r}) = -\sum_{(i,j)} C_{ij}/r_{ij}^{\;6} \tag{3}$$

respectively. The repulsion/dispersion parameters for our Estane potential are given in Table 3, along with the source for the interaction parameters. The large majority of parameters are taken from our quantum-chemistry-based potentials for polyethylene,[26] poly(ethylene oxide),[17] polystyrene,[16] and HMX[12] that have been successfully employed in simulations of those materials. The nonaromatic carbon, oxygen, and hydrogen parameters are based on earlier work of Sorensen et al.[27] For Estane, it was necessary to establish nonbonded interactions that accurately describe hydrogen bonding of the hydrogen atom pendant to the urethane nitrogen atom with the carbonyl oxygen ($O_D\cdots H_n$) and urethane nitrogen ($N\cdots H_n$) atoms. We also needed to establish the ability of our nonbonded potential to reproduce strong electrostatic interactions between carbonyl and amine groups. For this purpose, we carried out the quantum chemistry studies of the DMA and DMK complexes shown in Figure 4 and described above. The $O\cdots H_n$ and $N\cdots H_n$ repulsion/dispersion parameters (Table 3) were adjusted to give the best representation of the quantum chemistry binding energies for the DMA−DMK and $(DMA)_2$ complexes. As shown in Figure 5, good agreement was obtained. Figure 5 also reveals that the force field does a good job for binding in the $(DMK)_2$ complex, as well as non-hydrogen-bonding configuration of the $(DMA)_2$ complex.

TABLE 2: Partial Atomic Charges for Estane and Estane Model Compounds

atom	charge type	C-1	C-2	C-3	C-4	C-5	C-6	C-7	C-8	C-9	polymer
C_D		0.833	0.867	0.879	0.747	**0.762**	0.772	**0.829**		**0.959**	0.848
C	1		0.273	**0.026**				0.246		0.407	0.028
C	2			**0.192**							0.188
C	3				−0.151	**−0.534**				**−0.610**	−0.532
C	4					0.520				**0.317**	0.318
C	5								**−0.848**		−0.854
C_a	1						**−0.168**	**−0.166**	−0.152		−0.173
C_a	2						**0.307**	**0.307**			0.30
C_a	3								**0.281**		0.28
O_D		−0.522	−0.530	−0.530	−0.522	**−0.520**	−0.497	**−0.509**		**−0.571**	−0.542
O		−0.333	−0.443	−0.413	−0.418	**−0.336**	−0.272	**−0.436**		**−0.546**	−0.442
N							**−0.625**	**−0.670**			−0.67
H	1		0.009	**0.056**				0.003		−0.030	0.046
H	2			**−0.021**							−0.03
H	3				0.068	**0.125**				**0.145**	0.126
H	4					−0.087				**−0.072**	−0.075
H	5								**0.238**		0.23
H_n							**0.306**	**0.332**			0.319
H_a							**0.145**	**0.143**	0.133		0.137
$C_m{}^a$	1	−0.818	−0.925	−0.941							
$C_m{}^a$	2	−0.276			−0.176	−0.268	−0.410				
$C_m{}^a$	3		−0.220	−0.162	−0.114	−0.399		−0.110		−0.288	
$H_m{}^a$	1	0.225	0.251	0.254							
$H_m{}^a$	2	0.147			0.127	0.145	0.178				
$H_m{}^a$	3		0.069	0.039	0.039	0.088		0.040		0.082	

[a] Charges for terminating methyl groups. $C_m(1)$ is a methyl carbon bonded to C_D. $C_m(2)$ is a methyl carbon bonded to O. $C_m(3)$ is a methyl carbon bonded to a methylene carbon.

III. Bonded Force Field Parameters

A. Valence Bonds and Bends. The potential energy of valence bonds and bends was represented in our potential as

$$U_{\mathrm{bond}}(\mathbf{r}) = \sum_{(i,j)} \frac{1}{2} K_{\mathrm{bond}} (r_{ij} - r_0)^2 \tag{4}$$

$$U_{\mathrm{bend}}(\mathbf{r}) = \sum_{(i,j,k)} \frac{1}{2} K_{\mathrm{bend}} (\theta_{ijk} - \theta_0)^2 \tag{5}$$

respectively, where the sums are over all bonds and bends. The bond and bend force constants, K_{bond} and K_{bend}, for each type of valence bond and bend were taken from our previous work and work of Boyd,[28] Smith and Boyd,[29] and Sorensen et al.[27] These values are summarized in Table 4. Using the repulsion/dispersion parameters given in Table 3 along with the partial atomic charges in Table 2, we determined the valence geometry for the lowest-energy conformation of each Estane model compound using K_{bond} and K_{bend} values given in Table 4 and initial guesses for equilibrium bond lengths, r_0, and bond angles, θ_0, for each type of bond and bend by performing a molecular mechanics geometry optimization for each compound. Values of r_0 and θ_0 were adjusted to provide the best agreement between molecular mechanics and quantum chemistry (B3LYP/aug-cc-pvdz) geometries for these compounds. The optimal values of r_0 and θ_0 for each type of bond and bend and a comparison of average values (averaged over all occurrences in a given compound) for bond lengths and valence bend angles for representative compounds are given in Table 4.

B. Improper Torsions. The potential energy for improper torsions (out-of-plane bending) interactions at planar (sp^2-hybridized) atomic centers was represented with the function

$$U_{\mathrm{improper}}(\mathbf{r}) = \sum_{(i,j,k,l)} \frac{1}{2} K_{\mathrm{improper}} \delta_{ijk*l}{}^2 \tag{6}$$

TABLE 3: Repulsion and Dispersion Parameters for Estane and Estane Model Compounds

pair[a]	A_{ij} (kcal mol^{-1})	B_{ij} (Å^{-1})	C_{ij} (kcal mol^{-1} Å^6)	source
C···C	14 976	3.090	640.8	17, 26, 27
O···O	75 845	4.063	398.9	17, 27
H···H	2 650	3.740	27.4	17, 26, 27
C_a···C_a	78 998	3.600	519.0	16
H_a···H_a	2 384	3.740	24.6	16
N···N	60 834	3.780	500.0	12
H_n···H_n	2 650	3.740	27.4	set equal to H···H
C···O	33 702	3.577	505.6	17, 27
C···H	4 320	3.415	138.2	17, 26, 27
C···C_a	34 396	3.345	576.7	16
C···H_a	4 097	3.415	131.1	16
C···N	30 184	3.435	566.0	12
C···H_n	4 320	3.415	138.2	set equal to C···H
O···H	14 176	3.902	104.5	17, 27
O···C_a	77 405	3.832	455.0	combining rules[b]
O···H_a	13 447	3.902	99.1	combining rules[b]
O···N	67 926	3.921	446.6	12
O···H_n	24 492	4.613	104.5	this work
H···C_a	4 097	3.415	131.1	16
H···H_a	2 513	3.740	26.0	16
H···N	12 696	3.760	117.0	12
H···H_n	2 650	3.740	27.4	set equal to H···H
C_a···H_a	3 888	3.415	124.4	16
C_a···N	69 324	3.690	509.4	combining rules[b]
C_a···H_n	4 097	3.415	131.1	set equal to H···C_a
H_a···N	12 043	3.760	111.0	combining rules[b]
H_a···H_n	2 513	3.740	26.0	set equal to H···H_a
N···H_n	21 553	4.603	117.0	this work

[a] For determination of repulsion/dispersion parameters, O_D is assumed to be identical to O and C_D to C. [b] $A_{ij} = (A_{ii}A_{jj})^{1/2}$; $B_{ij} = (B_{ii} + B_{jj})/2$; $C_{ij} = (C_{ii}C_{jj})^{1/2}$.

where δ_{ijk*l} is the angle between the j−l bond and the i−j−k plane and the sum is over all combinations of *i*, *k*, and *l* centered at each planar center *j*. In addition to the anticipated improper torsions centered on aromatic carbons and carbonyl carbons, quantum chemistry revealed that the C_D−N(H)−C_a arrangement is also planar, necessitating the inclusion of urethane-nitrogen-

TABLE 4: Valence Bond and Bend Parameters for the Estane Force Field

bond types	K_{bond} (kcal mol^{-1} Å^{-2})	source	R_0 (Å)	compd	qc avg	mm avg
C−C	618	17, 26, 27	1.530	**C-5**	1.531	1.517
C_D-C	734	29	1.537	**C-5**	1.514	1.517
C−C_a	618	16	1.520	**C-8**	1.520	1.518
C−H	655	17, 26, 27	1.099	**C-5**	1.098	1.099
C−O	739	17, 27	1.433	**C-5**	1.441	1.451
C_D−O	749	29	1.350	**C-5**	1.355	1.365
C_D−O_D	1368	29	1.219	**C-5**	1.213	1.217
C_a−C_a	1102	16	1.391	**C-7**	1.400	1.400
C_a−H_a	727	16	1.088	**C-7**	1.090	1.089
C_a−N	672	28	1.423	**C-7**	1.410	1.420
N−C_D	734	set equal to C_D−C	1.399	**C-7**	1.372	1.374
N−H_n	720	28	1.023	**C-7**	1.011	1.011

bend type	K_{bend} (kcal mol^{-1} rad^{-2})	source	θ_0 (deg)	compd	qc avg	mm avg
H−C−H	77	17, 26, 27	107.1	**C-5**	108.3	107.9
H−C−C	86	17, 26, 27	110.7	**C-5**	110.7	110.5
H−C−C_D	86	29	108.8	**C-3**	107.8	107.6
C−C−O	119	17, 27	105.8	**C-5**	107.8	108.0
C−C_D−O	245	29	111.8	**C-5**	111.1	111.4
C−C_D−O_D	144	29	127.4	**C-5**	125.8	126.1
C_D−O−C	101	29	111.1	**C-3**	115.9	116.4
H−C−O	112	27	107.5	**C-5**	108.8	109.9
O−C_D−O_D	144	29	120.8	**C-5**	123.0	122.5
C−C−C	105	17, 26, 27	113.8	**C-5**	112.5	111.8
C_D−C−C	105	set equal to C−C−C	119.3	**C-5**	113.8	114.3
C_a−C−H	86	16	108.6	**C-8**	109.0	108.9
C_a−C_a−H_a	72	16	120.0	**C-8**	119.7	119.8
C_a−C_a−C_a	144	16	120.0	**C-8**	119.7	120.0
C_a−C_a−N	144	28	120.0	**C-7**	120.3	120.3
C_a−N−C_D	144	28	128.9	**C-7**	128.6	131.8
C_a−N−H_n	86	28	114.2	**C-7**	116.6	115.9
N−C_D−O_D	144	28	126.0	**C-7**	127.0	129.4
N−C_D−O	119	28	106.6	**C-7**	108.7	105.2
C−C_a−C_a	101	16	120.0	**C-8**	120.8	120.0
C_D−N−H_n	86	28	116.9	**C-7**	114.8	112.2
C_a−C−C_a	105	28	113.0	**C-8**	114.0	114.3

TABLE 5: Improper Torsion Parameters for the Estane Force Field

o-o-p bending type	$K_{improper}$ (kcal mol^{-1} rad^{-2})	source
C−C_D−O*O_D	51.8	29
C−C_D−O_D*O	0	
O−C_D−O_D*C	0	
C_a−C_a−C_a*N[a]	74.3	this work
C_a−C_a−C_a*H_a	36.5	16
C_a−N−C_D*H_n	28.8	28
O−C_D−N*O_D[a]	86.4	this work
C_a−C_a−C_a*C	74.3	this work

[a] Determined from the out-of-plane bending energy of a methyl group or amine group from the plane of the phenyl ring in toluene or aniline at the B3LYP/aug-cc-pvdz//MP2/aug-cc-pvdz level with a fixed phenyl geometry.

centered out-of-plane bending interactions. The out-of-plane bending force constants, taken from previous work, are tabulated in Table 5.

C. Dihedral Potential. The unique dihedrals in Estane are depicted in Figure 2. Each of these dihedral types occurs in at least one of the model Estane compounds investigated, as illustrated in Figure 3. Using the nonbonded parameters given in Table 3, the partial atomic charges given in Table 2, the valence bond and bend parameters given in Table 4, improper torsion parameters given in Table 5, and dihedral potentials of the form

$$U_{dihedral}(\mathbf{r}) = \sum_{(i,j,k,l)} \sum_{n} \frac{1}{2} K_{dihedral}{}^{n}[1 - \cos(n\phi_{ijkl})] \quad (7)$$

where the sum is over all dihedrals involving only backbone atoms, we determined the conformational energy of the important conformers of each model compound by performing a complete molecular mechanics geometry optimization. A similar procedure was followed for saddle points between important conformers and nonstationary points except that instead of a full geometry optimization one or more dihedrals was constrained at the angle obtained from quantum chemistry. The dihedral force constants, $K_{dihedral}{}^{n}$, were adjusted to give the best agreement between molecular mechanics and quantum chemistry for the conformational energy (MP2/aug-cc-pvDZ) and conformational geometry (B3LYP/aug-cc-pvDZ) for the important conformers and saddle points for each model compound. Molecular mechanics and quantum chemistry conformational energies and geometries for low-energy conformers and rotational energy barriers are compared in Table 1. In addition to stationary points shown in Table 1, nonstationary points with constrained dihedral angles were used in fitting the dihedral potential. A comparison between molecular mechanics and quantum chemistry for these points is shown in the conformational energy maps for each compound below. The resulting optimized dihedral force constants are given in Table 6. Below we discuss the conformational characteristics and agreement between molecular mechanics and quantum chemistry for each model compound.

TABLE 6: Dihedral Parameters for the Estane Force Field

backbone torsions	K_1[a]	K_2[a]	K_3[a]	K_4[a]	K_5[a]	K_6[a]	K_8[a]
C−C_D−O−C	−2.244	11.365	−0.635				
C_D−O−C−C	0.337	−0.206	0.217	0.121			
O−C−C−C	−0.331	−0.511	−3.318	−0.130	0.104	−0.052	
C−C−C−C	−0.948	−0.659	−3.067				
C_a−C−C_a−C_a		0.055		0.077			−0.044
C_a−C_a−N−C_D		2.486		0.167			
C_a−N−C_d−O	4.848	13.618	−5.293			1.071	
O−C_D−C−C	−0.756	0.377	−0.091	0.016	0.053		
C_D−C−C−C	0.112	−0.229	−2.475	0.039	0.231	0.562	
N−C_D−O−C	−1.370	8.992	−0.186				
C_a−C_a−C_a−C_a[b]		25.000					

[a] Given in kcal mol^{-1}. [b] Taken from ref 36.

*Methyl Acetate (**C-1**), Ethyl Acetate (**C-2**), and Propyl Acetate (**C-3**).* As can be seen from Table 1 and Figure 6, the molecular mechanics force field is able to reproduce accurately the energies and geometries of the important conformers and saddle points for the acetate model compounds. On the basis of our experience for related compounds, for which we have conducted extensive studies of the influence of basis set size and treatment of electron correlation on conformational geometries and energies,[17,30,31] we estimate the uncertainty in the conformer energies obtained from quantum chemistry to be ±0.3 kcal mol^{-1} and uncertainties in rotational energy barriers to be ±0.5 kcal mol^{-1}. With the exception of the $\{\phi_1\phi_2\phi_3\}$ = tg$^+$g$^-$ conformer[32] of propyl acetate, for which the molecular mechanics energy lies within 0.5 kcal mol^{-1} of the quantum chemistry energy, all molecular mechanics conformer energies lie within the estimated error bars of their respective quantum chemistry values for the acetate model compounds. The stability of the tg$^+$g$^-$ conformer (both from quantum chemistry and molecular mechanics) indicates

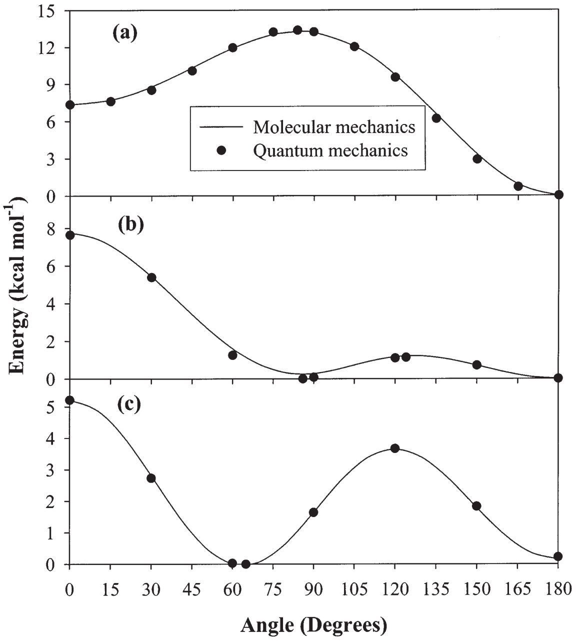

Figure 6. Conformational energy of (a) methyl acetate, (b) ethyl acetate, and (c) propyl acetate as a function of dihedral angle for dihedral types 1, 2, and 3, respectively, from quantum chemistry (symbols) and molecular mechanics (lines).

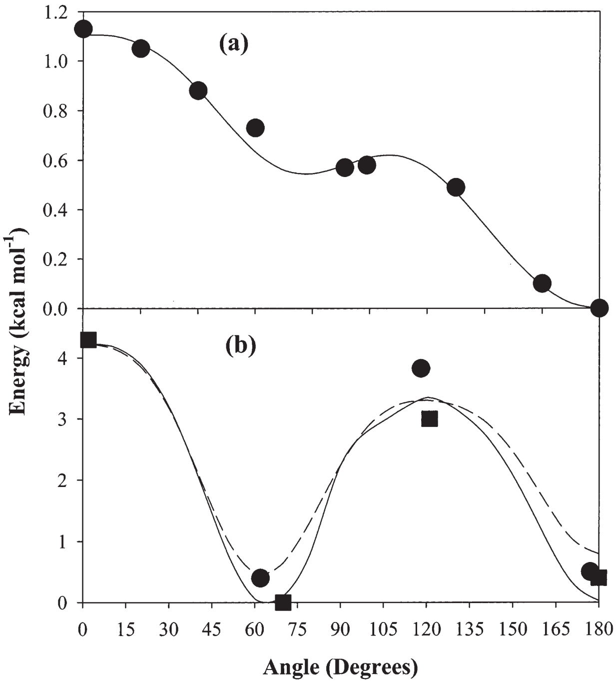

Figure 7. Conformational energy of (a) methyl propanoate and (b) methyl butanoate as a function of dihedral angle for dihedral type 8 and 9, respectively, from quantum chemistry (symbols) and molecular mechanics (lines). For methyl butanoate, drives of ϕ_9 with ϕ_8 in the t (—, quantum chemistry = ■) and g (— — —, quantum chemistry = ●) states are shown.

that the pentane effect expected to be manifested in this conformation is small. We believe that this is due to offsetting of unfavorable steric interactions by favorable electrostatic interactions between O_D and the methyl group. Examination of Figure 6a reveals a strong preference of ϕ_1 for the t conformation; the c state is too high in energy to have significant population at reasonable temperatures. Consequently, conformations of ϕ_2 and ϕ_3 were explored for ϕ_1 = t only. Rotation about ϕ_2 reveals nearly isoenergetic t and g states separated by a low barrier. The g states are significantly distorted from the ±60°–65° typically found in alkanes and ethers. The g energy, g–t barrier, and distortion of the g geometry are in good agreement with values obtained from spectroscopic studies of ethyl acetate[33] and ethyl formate.[34] As with ϕ_2, the t and g states for ϕ_3 are also nearly isoenergetic, but they have a significantly larger barrier between them. The g geometry for ϕ_3 is more typical of an alkane or ether.

*Methyl Propanoate (**C-4**) and Methyl Butanoate (**C-5**).* Table 1 and Figure 7 reveal that the molecular mechanics force field accurately reproduces the geometries and energies of the low-energy conformers and rotational energy barriers for methyl propanoate and methyl butanoate. Rotation about ϕ_8 reveals that the dihedral is quite labile; the maximum conformation energy (at c) is only about 1 kcal mol^{-1} greater than the minimum at t. We also observe a shallow g state in methyl propanoate with an energy in good agreement with estimates obtained from spectroscopic studies.[35] We note that the empirical force field for ester-group-containing polymers parametrized by one of us to reproduce available experimental data on conformational energies, geometries, and vibrational frequencies for model esters captures reasonably well the g energy and g–t barrier in methyl propanoate.[29] However, this earlier empirical potential yields a c barrier that is significantly higher than that indicated by quantum chemistry, yielding a much less labile dihedral. This discrepancy illustrates the necessity of determining all conformer and saddle point energies when fitting dihedral potentials and hence the utility of quantum chemistry studies of model compounds, which are often the only source of accurate conformational energies. Rotation about ϕ_9 reveals a preference for the g state with moderate barriers between g and t conformations. The stability of the $\{\phi_1\phi_8\phi_9\}$ = tg$^+$g$^-$ conformer of methyl propanoate again indicates the absence of a strong pentane effect, due here to the small steric size of the backbone oxygen atom and favorable electrostatic interactions between the methyl group and the oxygen, analogous to effects observed in simple ethers.[17]

*Methyl-N-phenyl Carbamate (**C-6**) and Ethyl-N-phenyl Carbamate (**C-7**).* Figure 8 and Table 1 show that the molecular mechanics potential accurately reproduces the conformational energies and geometries of the low-energy conformers and rotational energy barriers in methyl-*N*-phenyl carbamate and ethyl-*N*-phenyl carbamate. The conformational energy of methyl-*N*-phenyl carbamate as a function of dihedral angle for dihedral type 6 is shown in Figure 8a. Symmetry restricts us to using n = 2, 4, and 8 in the dihedral potential (eq 7) for dihedral type 6. Rotation of the phenyl ring about ϕ_6 reveals a moderate barrier at 90°. In contrast, rotation about dihedral type 7 (Figure 8b) has a very high barrier between the t (preferred) and c conformations, precluding rotational isomerization between these states. Figure 8c shows that energetics of rotation about dihedral type 10 are very similar to those for the chemically similar dihedral type 1 (see discussion of acetate compounds above). Finally, Figure 8d shows that dihedral parameters obtained for dihedral type 2 from the acetate compounds reproduce well the conformational energetics for rotation about this dihedral type in ethyl-*N*-phenyl carbamate.

*Biphenylmethane (**C-8**).* Figure 9 is a conformational energy map for rotation about the ϕ_5 dihedrals (labeled ϕ_5^a and ϕ_5^b) in biphenylmethane. Because of symmetry, it is only necessary to consider 0° ≤ ϕ_5 ≤ 90°. Symmetry also restricts us to using n = 2, 4, and 8 in the dihedral potential (eq 7) for dihedral type

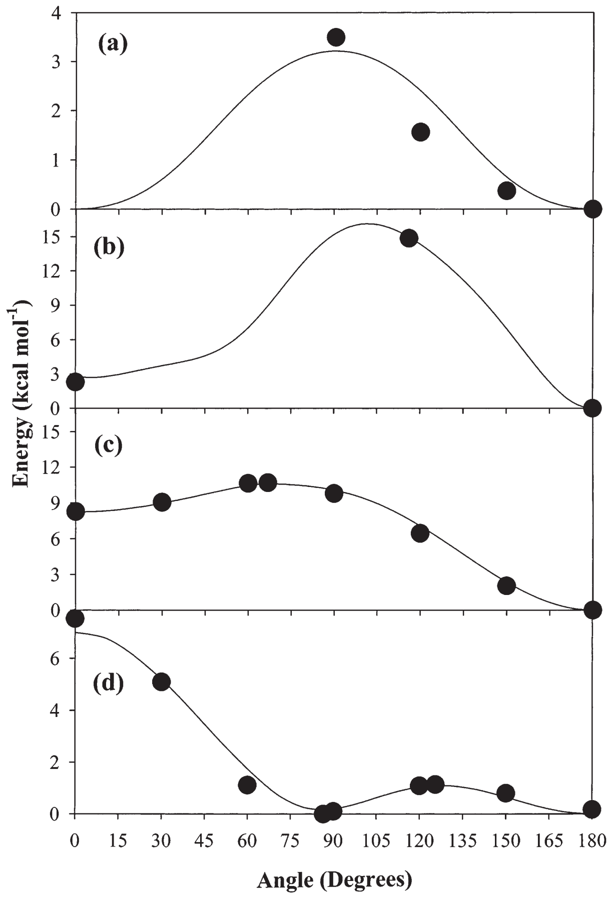

Figure 8. Conformational energy of methyl-*N*-phenyl carbamate and ethyl-*N*-phenyl carbamate from quantum chemistry (symbols) and molecular mechanics (lines): (a) methyl-*N*-phenyl carbamate, rotation of ϕ_6 for $\{\phi_7\phi_{10}\}$ = tt; (b) methyl-*N*-phenyl carbamate, rotation of ϕ_7 for $\{\phi_6\phi_{10}\}$ = tt; (c) methyl-*N*-phenyl carbamate, rotation of ϕ_{10} for $\{\phi_6\phi_7\}$ = tt; (d) ethyl-*N*-phenyl carbamate, rotation of ϕ_2 for $\{\phi_6\phi_7\phi_{10}\}$ = ttt.

5. The conformational energy surface is nearly isoenergetic for $\phi_5{}^b > 90° - \phi_5{}^a$. The energy rises quickly as the $\{\phi_5{}^a\phi_5{}^b\}$ = cc saddle point is approached due to steric interactions. In contrast the 90°90° and 0°90° saddle points are very low in energy. The level of agreement between quantum chemistry and molecular mechanics for conformational energies of biphenylmethane is somewhat poorer than that for the other compounds investigated. However, the uncertainties in the quantum chemistry energies for biphenylmethane are likely to be greater because of difficulties in reproducing phenyl−phenyl interactions at the level of theory employed in our study.[16,36]

*Hexanedioic Acid Diethyl Ester (**C-9**).* Figure 10 shows a drive about the dihedral ϕ_4 in hexanedioic acid diethyl ester. Quantum chemistry geometries and energies for the low-energy conformers and rotational barriers are well reproduced by the force field. Conformational energetics for rotation about ϕ_4 are typical of those found in simple alkanes.[30]

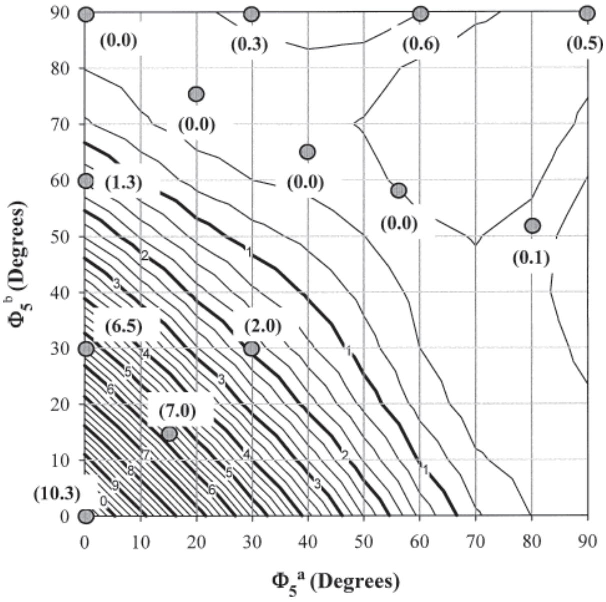

Figure 9. Conformational energy map for biphenylmethane for rotation about the type 5 dihedral angles. Energy contours are spaced at 0.25 kcal mol^{-1}. Points are from quantum chemistry with relative conformational energies shown in parentheses.

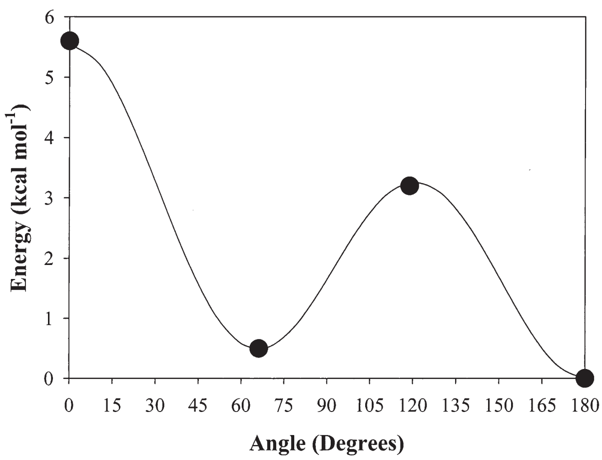

Figure 10. Conformational energy of hexanedioic acid diethyl ester as a function of dihedral angle for dihedral type 4 from quantum chemistry (symbols) and molecular mechanics (line).

IV. Validation

We have validated our potential by comparing thermodynamic properties and crystal lattice parameters for various model

TABLE 7: Comparison of Thermodynamic and Structural Data for Model Compounds from Molecular Dynamics Simulations and Experiment

compound	property	T (K)	expt	simul	expt ref
BPM[a]	liquid density (kg m^{-3})	299	1001	1020	41
HADE[b]	liquid density (kg m^{-3})	299	979	987	41
MDI[c]	lattice parameters a, b, c (Å)	258	5.157, 9.800,31.472	5.280, 9.831,30.625	37
	lattice parametersα, β, γ (deg)		90.0, 90.0,93.9	90.0, 90.0,91.0	
	unit cellvolume (Å^3)		1587	1590	

[a] Biphenylmethane, compound **C-8**, Figure 3. C−C$_a$ and C$_a$−C$_a$ bonds were constrained to 1.54 and 1.43 Å, respectively, values that are slightly larger than the average quantum chemistry values for these bonds given in Table 4. [b] Hexanedioic acid dipropyl ester. [c] Dimethyl 4,4′-methylenebis(phenylcarbamate).

compounds obtained from molecular dynamics (MD) simulations using our quantum-chemistry-based potential with available experimental data. MD simulations of liquid-phase biphenylmethane (BPM) and hexanedioic acid dipropyl ester (HADE, chemical structure $CH_3-C_2H_4-CO_2-C_4H_8-CO_2-C_2H_4-CH_3$) were performed at atmospheric pressure. Each system consists of 125 molecules. We also conducted simulations of the crystalline phase of dimethyl 4,4′-methylenebis(phenylcarbamate) (MDI). The MDI molecules (chemical structure $CH_3-CO_2-NH-C_6H_4-CH_2-C_6H_4-NH-CO_2-CH_3$) are representative of polyurethane hard segments and basically consist of our two **C-6** compounds (see Figure 3) connected through the phenyl rings by a methane group. MDI has a monoclinic structure with $P2_1/b$ space group symmetry ($Z = 4$), which has been well characterized by X-ray crystallography at 258 K.[37] We used a combined molecular dynamics/Monte Carlo approach[38] to perform *NpT* ensemble simulations in the fully flexible simulation cell. Initial configuration was obtained from experimental crystal structure.[37] Simulations were performed on a system containing 60 molecules, which corresponds to 15-($5 \times 3 \times 1$) unit cells. For both liquid and crystal simulations, Ewald summation[39] was used to account for long-range electrostatic interactions. A cutoff radius of 10.0 Å was used for all van der Waals interactions and the real part of the electrostatic interactions. The SHAKE algorithm[40] was used to constrain bond lengths, while bends, torsions, and out-of-plane dihedrals were kept unconstrained during the simulation. Equilibration runs over 1.0 ns were followed by 3.0 ns production runs. Integration time step was 1 fs. A comparison of properties from simulation and experiment[37,41] is summarized in Table 7. Very good agreement is seen for each compound investigated. The properties investigated are sensitive to intermolecular (nonbonded) interactions, indicating that the quantum chemistry potential accurately represents electrostatic, dispersion/repulsion, and hydrogen-bonding interactions in these compounds. The crystal structure of MDI is particularly sensitive to the intermolecular electrostatic interactions, including hydrogen bonding.

V. Summary

We have presented here a complete bonded and nonbonded force field for a series of model compounds for Estane based upon extensive ab initio electronic structure calculations of geometries and energies. This potential can be used for atomistic simulations of Estane and is anticipated to reproduce conformational energetics with uncertainties comparable to those in quantum chemistry data used to parametrize the potential. The force field is also applicable to a wide variety of poly(urethanes) and poly(esters) for which the investigated compounds are representative.

Acknowledgment. Utah participants in this research acknowledge support for this work from Los Alamos National Laboratory through Contract 349630010139. D.B., C.A., and G.D.S. are funded by the University of Utah Center for the Simulation of Accidental Fires and Explosions (C-SAFE), funded by the Department of Energy, Lawrence Livermore National Laboratory, under Subcontract B341493. T.D.S. is supported by the Los Alamos ASCI/HE effort.

References and Notes

(1) Estane Thermoplastic Polyurethanes. www.estane.com.
(2) Woods, G., Ed. *The ICI Polyurethanes Handbook*, 2nd ed.; J. Wiley and Sons: New York, 1990.
(3) Hepburn, C., Ed. *Polyurethane Elastomers*, 2nd ed.; Elsevier: New York, 1992.
(4) Quigley, F.; Bryan, K.; Buggy, M.; Birkinshaw, C. *Key Eng. Mater.* **1996**, *118*, 313.
(5) de Groot, J. H.; Nijenhuis, A. J.; Bruin, P.; Pennings, A. J.; Veth, R. P. H.; Klompmaker, J.; Jansen H. W. B. *Colloid Polym. Sci.* **1990**, *268*, 1073.
(6) Tanzi, M. C.; Ambrosio, L.; Nicolais, L.; Lannace, S.; Ghislanzoni, L.; Mambrito, B. *Clin. Mater.* **1991**, *8*, 57.
(7) Salazar, M. R.; Pack, R. T. *J. Polym. Sci, Part B: Polym. Phys.* **2002**, *40*, 192.
(8) Hoffman, D. M. *J. Appl. Polym. Sci.* **2002**, *83*, 1009.
(9) Christenson, C. P.; Harthcock, M. A.; Meadows, M. D.; Spell, H. L.; Howard, W. L.; Creswick, M. W.; Guerra, R. E.; Turner, R. B. *J. Polym. Sci., Part B: Polym. Phys.* **1986**, *24*, 1401.
(10) Garrett, J. T.; Lin, J. S.; Runt, J. *Macromolecules* **2002**, *35*, 161 and references therein.
(11) Bedrov, D.; Smith, G. D.; Douglas, J. F. *Europhys. Lett.* **2002**, *59*, 384.
(12) Smith, G. D.; Baharadwaj, R. K. *J. Phys. Chem. B* **1999**, *103*, 3570.
(13) Bedrov, D.; Smith, G. D.; Sewell, T. *J. Chem. Phys.* **2000**, *112*, 7203. Bedrov, D.; Smith G. D.; Sewell, T. D. *Chem. Phys. Lett*. **2000**, *324*, 64.
(14) Bedrov, D.; Ayyagari, C.; Smith, G. D.; Sewell, T. D.; Menikoff, R.; Zaug, J. M. *J. Comput.-Aided Mater. Des.* **2002**, *8,* 77. Sewell, T. D.; Menikoff, R.; Bedrov, D.; Smith, G. D. *J. Chem. Phys.*, in press.
(15) Byutner, O. G.; Smith, G. D. *Macromolecules* **2000**, *33*, 4264.
(16) Ayyagari, C.; Bedrov, D.; Smith, G. D. *Macromolecules* **2000**, *33*, 6194.
(17) Smith, G. D.; Jaffe, R. L.; Yoon, D. Y. *J. Phys. Chem.* **1993**, *97*, 12752.
(18) Smith, G. D.; Borodin, O.; Bedrov, D. *J. Phys. Chem. A* **1998**, *102*, 10318.
(19) Smith, G. D.; Paul, W. *J. Phys. Chem. A* **1998**, *102*, 1200.
(20) Frisch, M. J.; Trucks, G. W.; Schlegel, H. B.; Scuseria, G. E.; Robb, M. A.; Cheeseman, J. R.; Zakrzewski, V. G.; Montgomery, J. A., Jr.; Stratmann, R. E.; Burant, J. C.; Dapprich, S.; Millam, J. M.; Daniels, A. D.; Kudin, K. N.; Strain, M. C.; Farkas, O.; Tomasi, J.; Barone, V.; Cossi, M.; Cammi, R.; Mennucci, B.; Pomelli, C.; Adamo, C.; Clifford, S.; Ochterski, J.; Petersson, G. A.; Ayala, P. Y.; Cui, Q.; Morokuma, K.; Malick, D. K.; Rabuck, A. D.; Raghavachari, K.; Foresman, J. B.; Cioslowski, J.; Ortiz, J. V.; Stefanov, B. B.; Liu, G.; Liashenko, A.; Piskorz, P.; Komaromi, I.; Gomperts, R.; Martin, R. L.; Fox, D. J.; Keith, T.; Al-Laham, M. A.; Peng, C. Y.; Nanayakkara, A.; Gonzalez, C.; Challacombe, M.; Gill, P. M. W.; Johnson, B. G.; Chen, W.; Wong, M. W.; Andres, J. L.; Head-Gordon, M.; Replogle, E. S.; Pople, J. A. *Gaussian 98*, revision A.1; Gaussian, Inc.: Pittsburgh, PA, 1998.
(21) Becke, A. D. *J. Chem. Phys*. **1993**, *98*, 5648. Lee, C.; Yang, W.; Parr, R. G. *Phys. Rev. B* **1988**, *37*, 785.
(22) Woon, D. E.; Dunning, T. H. *J. Chem. Phys.* **1994**, *100*, 2975.
(23) Woon, D. E.; Dunning, T. H. *J. Chem. Phys.* **1993**, *98,* 1358.
(24) Boys, S. F.; Bernardi, F. *Mol. Phys.* **1970**, *19*, 553.
(25) The most representative compounds for a given atom type were chosen as those in which the atom(s) of that type was furthest removed from the termination groups for that compound.
(26) Smith, G. D.; Yoon, D. Y.; Zhu, W.; Ediger, M. D. *Macromolecules* **1994**, *27*, 5563.
(27) Sorensen, R. A.; Liau, W. B.; Kesner, L.; Boyd, R. H. *Macromolecules* **1988**, *21*, 200.
(28) Boyd, R. H. Private communication (from the molecular simulation package MOLBYD).
(29) Smith, G. D.; Boyd, R. H. *Macromolecules* **1990**, *23*, 1527.
(30) Smith, G. D.; Jaffe, R. L. *J. Phys. Chem.* **1996**, *100*, 9624.
(31) Borodin, O.; Smith, G. D. *J. Phys. Chem. B* **2003**, *107*, 6801.
(32) States for dihedrals with three minima are denoted as follows: $0° < g^+ \leq 120°$; $120° < t \leq 240°$; $240° < g^- \leq 360°$. States for dihedrals with two minima are denoted as $90° < t \leq 270°$; $-90° < c \leq 90°$.
(33) George, W. O.; Hassid, D. V.; Maddams, W. F. *J. Chem. Soc., Perkins Trans. 2* **1972**, 1798.
(34) Riveros, J. M.; Wilson, E. B. *J. Chem. Phys.* **1967**, *46*, 4605.
(35) Moravie, R.-M.; Corset, J. *Chem. Phys. Lett.* **1974**, *26*, 210.
(36) Jaffe, R. L.; Smith, G. D. *J. Chem. Phys*. **1996**, *105*, 2780.
(37) Gardner, K. H.; Blackwell, J. *Acta Crystallogr.* **1980**, *B36*, 1972.
(38) Sewell, T. D.; Menikoff, R.; Bedrov, D.; Smith, G. D. *J. Chem. Phys*., in press.
(39) Allen, M. P.; Tildesley, T. J. *Computer Simulations of Liquids*; Oxford University Press: Oxford, U.K., 1987.
(40) Ryckaert, J.; Ciccotti, G.; Berendsen, H. J. C. *J. Comput. Phys*. **1977**, *23*, 327.
(41) *CRC Handbook of Chemistry and Physics*, 83rd ed. (electronic version); CRC Press: Boca Raton, FL; http://www.hbcpnetbase.com.